Chem

CellPress
OPEN ACCESS

Article

A room-temperature-stable electride and its reactivity: Reductive benzene/pyridine couplings and solvent-free Birch reductions

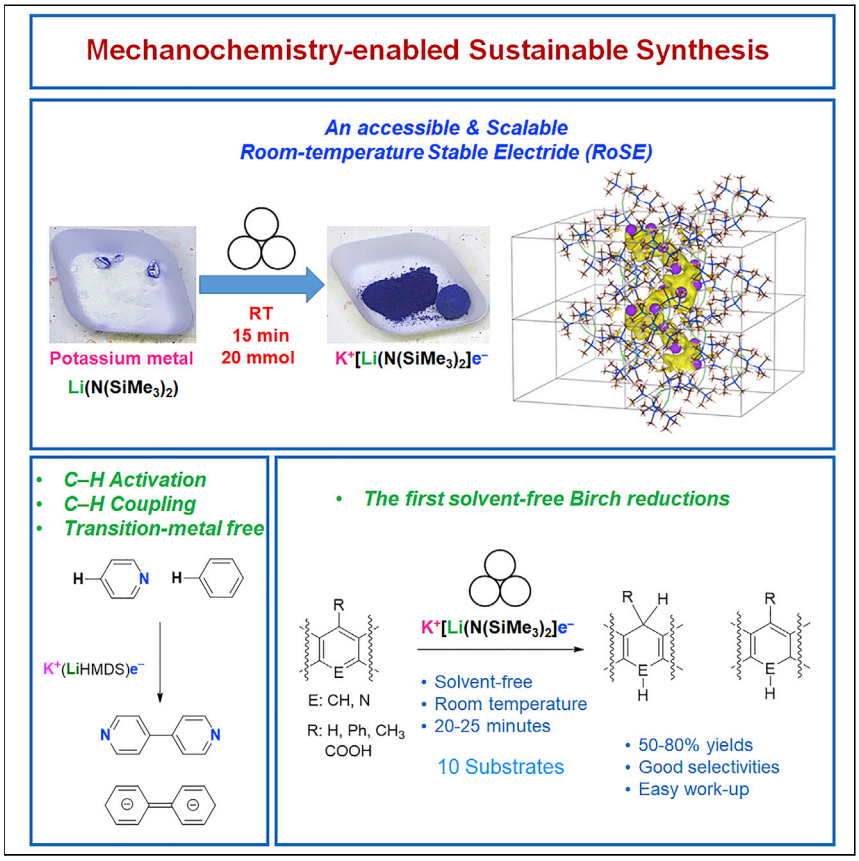

Organic synthesis is playing underpinning roles in industries and academic research. But from a sustainability perspective, current organic synthesis protocols are criticized for the usage of petrochemical-derived solvents and precious-metal reagents. Herein, we report an unprecedented facile preparation of an enabling reagent, namely a room-temperature-stable electride (RoSE). Utilizing the RoSE reagent, we phase out transition-metal reagents and solvents from two notoriously unsustainable organic reactions: (1) benzene and pyridine C–H activation and C–C coupling and (2) arene Birch reduction.

Nathan Davison, James A. Quirk, Floriana Tuna, ..., Marina Freitag, James A. Dawson, Erli Lu

floriana.tuna@manchester.ac.uk (F.T.)
cm2025@bath.ac.uk (C.L.M.)
james.dawson@newcastle.ac.uk (J.A.D.)
erli.lu@newcastle.ac.uk (E.L.)

Highlights

Use mechanical forces (mechanochemistry) to enable sustainable chemical synthesis

An unprecedentedly accessible room-temperature stable electride (RoSE)

RoSE-mediated benzene and pyridine C–H activation and C–C coupling

RoSE-mediated solvent-free Birch reduction

Davison et al., Chem 9, 576–591
March 9, 2023
https://doi.org/10.1016/j.chempr.2022.11.006

CellPress
OPEN ACCESS

Chem

Article

A room-temperature-stable electride and its reactivity: Reductive benzene/pyridine couplings and solvent-free Birch reductions

Nathan Davison,[1,6] James A. Quirk,[1,6] Floriana Tuna,[2,*] David Collison,[2] Claire L. McMullin,[3,*] Hannes Michaels,[1,4] George H. Morritt,[5] Paul G. Waddell,[1] Jamie A. Gould,[1] Marina Freitag,[1] James A. Dawson,[1,*] and Erli Lu[1,7,8,*]

SUMMARY

In this work, we report the synthesis of a room-temperature-stable electride (RoSE) reagent, namely $K^+(LiHMDS)e^-$ (1) (HMDS: 1,1,1,3,3,3-hexamethyldisilazide), from accessible starting materials (potassium metal and LiHMDS) via mechanochemical ball milling at 20 mmol scale. Despite its amorphous nature, the presence of anionic electrons in 1, key diagnostic criteria for an electride, was confirmed by both experimental and computational studies. Therefore, by definition, 1 is an electride. Utilizing its anionic electrons, electride reagent 1 exhibited a versatile reactivity profile that includes (1) mediation of C–H activation and C–C coupling of benzene and pyridine and (2) mediation of solvent-free Birch reduction. This work proves the concept of facile mechanochemical synthesis of a room-temperature-stable electride, and it introduces electride 1 to the synthetic chemistry community as a versatile reagent.

INTRODUCTION

In the context of pursuing a sustainable future, significant research effort across the chemistry communities is being invested in developing new enabling reagents to facilitate challenging organic reactions, aimed at phasing out precious-metal catalysts, hazardous and expensive specialized reagents, and solvents.[1] Specifically, since Kekulé announced the groundbreaking aromaticity concept of benzene 150 years ago,[2] arene (including hetero-arene) transformations have been the cornerstones of organic chemistry, highlighted by several named reactions, e.g., Friedel-Crafts,[3] Birch,[4] Sandmeyer,[5] and Scholl.[6] However, as a result of the inherent stability of the arenes originating from their aromaticity, these arene transformations usually require harsh conditions, precious-metal catalysts, and pre-functionalized substrates.

In this work, we focus on two classic reactions: (1) direct C–H activation and C–C coupling of benzene and pyridine (archetypical arene and hetero-arene, respectively) and (2) Birch reduction. As the archetypical and most inert arene, direct benzene C–H activation and C–C coupling require harsh conditions, such as strong oxidants (e.g., hypervalent iodine)[7–9] and precious-metal catalysts (e.g., palladium catalysts) (Figure 1A).[10–12] Compared with these well-documented oxidative processes, *reductive* tandem benzene C–H activation and C–C coupling is unknown. The two most relevant precedents are trivalent yttrium-alkyl-mediated[13] and

THE BIGGER PICTURE

Minimizing energy consumption, pollution, and the usage of hazardous chemicals in organic synthesis is a grand scientific challenge. A sustainable vision of organic synthesis requires new reagents, the use of no precious metals or solvents, and the ability to perform challenging transformations under facile conditions. Herein, we report a new and accessible approach to a group 1 metal reagent featuring anionic electrons: an electride. Endowed with unique anionic electrons, electrides have great potential in synthetic chemistry, but the prospect is restrained by their inaccessibility and instability. This work provides the first accessible and scalable room-temperature-stable electride (RoSE). Our preliminary reactivity studies unveil the tip of the iceberg regarding the precious-metal-free RoSE's potential as a reagent, including benzene and pyridine C–H activation and C–C coupling, and the first solvent-free Birch reductions, which unlock a wealth of possibilities in sustainable organic synthesis.

divalent platinum-alkyl-mediated[14] benzene C–H activation and C–C coupling, both operating through a Brønsted acid-base mechanism, producing a biphenyl dianion. Very recently, electron-rich, low-valent main-group metal complexes have been reported to mediate reductive benzene C–H activation,[15,16] which requires sophisticated and bespoke main-group metal complexes. Conversely, *reductive* tandem pyridine C–H activation and C–C coupling, mediated by sodium metal producing 4,4′-bipyridine under harsh conditions (refluxing pyridine), was reported as early as 1868.[17] However, this reaction has been largely overlooked. The current bipyridine syntheses rely on homocoupling of halogenated pyridines catalyzed by Cu, Ni, or Pd catalysts.[18] A transition-metal-free reagent mediating facile benzene and pyridine tandem C–H activation and C–C coupling is highly desirable, but to the best of our knowledge, such a reagent is still unknown.

Birch reduction[19] converts arenes into cyclohexadienes. It is a classic organic reaction utilizing free anionic electrons (e.g., solvated electrons). Despite the wide applications of Birch reduction, its electron-rich reagents, such as the original and still prevailing group 1 metal-liquid ammonia (M-NH_3(l)) (M: Li, Na) condition,[20–22] present formidable technical and safety challenges (Figure 1B). Recent efforts have been directed toward phasing out the liquid ammonia via electrochemical,[23–25] photochemical,[26–28] and enzymatic[29] methods, as well as employing lithium/sodium metal in ammonia-free solvent systems (Figure 1B).[30–34] Nonetheless, there is still vast room for improvement regarding phasing out specialized photosensitizers, catalysts, enzymes, and last but not least, solvents. An ideal scenario is that an easily accessible electron-rich reagent can mediate solvent-free Birch reduction at room temperature in short reaction time, but such an enabling reagent is still unknown.

In such a context, we set our target to seek an easily accessible electron-rich reagent that can mediate benzene and pyridine C–H activation and C–C coupling, as well as solvent-free Birch reduction. As a prime candidate, electrides are a class of compounds and materials featuring trapped anionic electrons, which do not bind to any nucleus.[35–37] The anionic electrons endow the electrides with unusual physical properties, such as optical and magnetic, which have been intensively studied in the past decade with a view to applications in materials science.[37] As a reagent, the high reactivity of electrides has been exploited in a limited category of organic and inorganic reactions.[37] Specifically relevant to this work, an inorganic electride, namely dicalcium nitride $[Ca_2N]^+e^-$,[38] was reported to promote Birch reductions of polycyclic aromatic hydrocarbons (PAHs) in polar solvents (hexamethylphosphoramide [HMPA] and isopropanol [^{i}PrOH]) at elevated temperatures in 24 h, where the electride acted as an analog of solvated electrons.[39] In this case, only PAHs (not hetero-arenes, e.g., pyridine or acridine, or benzene or substituted benzene) were tested as substrates. Despite these reports utilizing electrides as reagents, they are still not well recognized by the synthetic chemistry community. This status can be explained by the low accessibility and often poor stability of the current electrides. Room-temperature-stable, inorganic electrides are synthesized via high-temperature (>600°C) calcination reduction of precursors with active metal (e.g., calcium shot),[37] such as $[Ca_2N]^+e^-$ (from Ca_3N_2 and Ca)[38] and an archetypical inorganic electride $[Ca_{24}Al_{28}O_{64}]^{4+}4e^-$ (from $12CaO{\cdot}7Al_2O_3$ and Ca).[40] Other than the electron-rich electrides synthesized from the harsh reduction methods, an electron-neutral Na_3N electride was recently synthesized via plasma-assisted nitridation of alkali metals.[41] Although not scalable from a synthetic chemistry perspective, high-pressure conditions have also been explored—mostly from theoretical approaches—to facilitate the formation of electrides,[36,37] including a recent report

[1]Chemistry, School of Natural and Environmental Sciences, Newcastle University, Newcastle upon Tyne NE1 7RU, UK

[2]Department of Chemistry and Photon Science Institute, University of Manchester, Oxford Road, Manchester M13 9PL, UK

[3]Department of Chemistry, University of Bath, Claverton Down, Bath BA2 7AY, UK

[4]Ångström Laboratory, Department of Chemistry, Uppsala University, Uppsala 75120, Sweden

[5]School of Mathematics, Statistics, and Physics, Newcastle University, Newcastle upon Tyne NE1 7RU, UK

[6]These authors contributed equally

[7]The name of E.L. in simplified Chinese characters is 陆而立

[8]Lead contact

*Correspondence:
floriana.tuna@manchester.ac.uk (F.T.),
cm2025@bath.ac.uk (C.L.M.),
james.dawson@newcastle.ac.uk (J.A.D.),
erli.lu@newcastle.ac.uk (E.L.)

https://doi.org/10.1016/j.chempr.2022.11.006

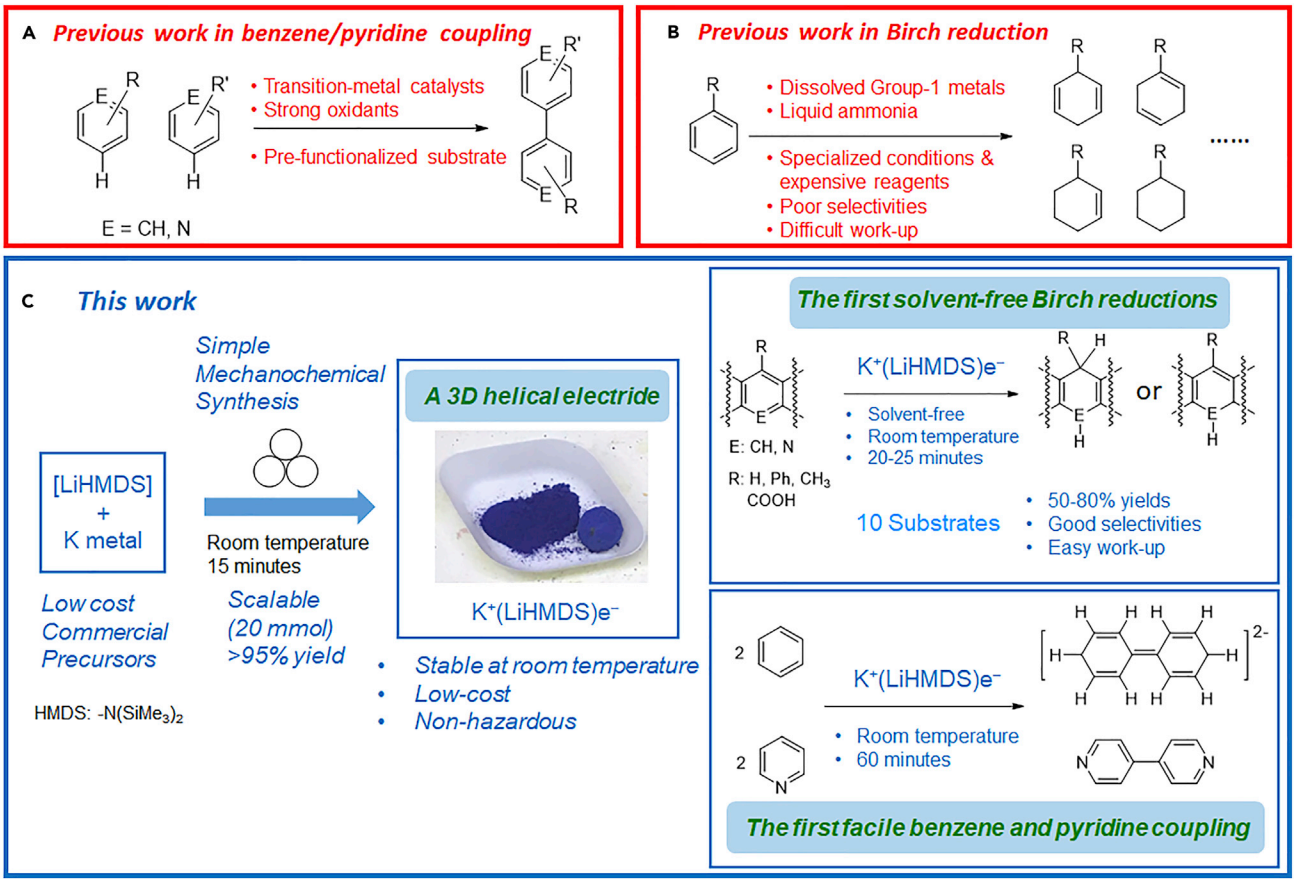

Figure 1. The state of the art and this work

(A) Previous work in benzene and pyridine coupling.

(B) Previous work in Birch reduction.

(C) This work: mechanochemical synthesis of a room-temperature-stable, 3D electride $K^+(LiHMDS)e^-$ (**1**) and its mediated solvent-free Birch reductions and facile benzene and pyridine coupling.

of a rare electron-deficient electride, Ca_5Pb_3, where pressure-induced electron accumulation was theoretically investigated.[42] Organic electrides, pioneered by the Dye group,[35] are synthesized by treating group 1 metals with crown-ethers or aza-crown-ethers at low temperatures. However, synthesizing and using organic electrides are extremely challenging. Only nine organic electrides have been synthesized since the 1980s,[35] and only two of these are stable at room temperature. Dye and co-workers reported one in 2005 by utilizing a specialized bespoke aza-cryptand ligand, which is difficult to synthesize.[43] During the preparation of this manuscript, Martin and co-workers reported the second room-temperature-stable electride (RoSE) from a serendipitous magnesium metal reduction of nickel(II) complexes,[44] where the electron was trapped in a $Mg_4(Bipy)_4$ (Bipy: 2,2′-bipyridine) framework. None of the reported electrides were prepared from low-cost precursors via a scalable and facile protocol, which hampers their use as reagents.

In this work, enabled by mechanochemical ball milling,[45] we report the first synthesis and characterization of a RoSE from low-cost starting materials via a scalable and easy protocol (20 mmol, 15 min). The electride, namely $K^+(LiHMDS)e^-$ (**1**) (HMDS: 1,1,1,3,3,3-hexamethyldisilazide), can promote facile tandem C–H activation and C–C coupling of benzene and pyridine, as well as the first solvent-free Birch

reductions (Figure 1C). Herein, we introduce **1** to the synthetic chemistry community as a versatile free-electron reagent.

RESULTS AND DISCUSSION

Synthesis and characterization of the electride K^+(LiHMDS)e^- (1)

Commercially available and low-cost lithium bis(trimethylsilyl)amide ([LiHMDS]; $310/mol) and potassium metal (K metal; $110/mol) were treated in a mechanochemical ball mill (Retsch MM400) at 30 Hz frequency for 15 min at room temperature. A homogeneous blue powder was obtained (Figure 2A). The synthesis of **1** is entirely reproducible and has been accomplished on the scale of 20 mmol. Once synthesized, **1** remains indefinitely stable at room temperature under argon (Ar) or nitrogen (N_2): the color and electroconductivity of **1** do not change under Ar or N_2 at room temperature for several weeks. However, despite the high thermal stability, electride **1** is extremely sensitive to trace amounts of moisture, oxygen, and proton sources. For instance, all the glassware contacting with **1** must be silylated with Me_3SiCl[46]; otherwise, the hydroxide (–OH) residues on the glass surface will induce **1**'s decomposition and cause the characteristic blue color to fade within 5 min, and it will lose its electroconductivity. The intense blue color of **1** is reminiscent of solvated anionic electrons in the Na-NH_3(l) system as Farbe centers (F centers), first observed by Sir Humphrey Davy over 200 years ago[47] and recently revisited by Jungwirth and co-workers.[48] The characteristic blue color was also observed in a few organic electrides,[49] indicating that the color could act as an intuitive sign of the presence of anionic electrons. Powder X-ray diffraction data reveal some indistinct peaks, but overall the material is amorphous (Figure S9). It is insoluble or reacts with all organic solvents we could test, and it decomposes into [LiHMDS] and K metal upon sublimation. Therefore, attempts to obtain its single-crystal structure were not successful. Gratifyingly, *ab initio* random structure searching (AIRSS)[46,50] enabled successful determination of the chemical formula of the blue powder as an electride: K^+(LiHMDS)e^- (**1**). The AIRSS method has been widely employed for searching for stable structures of materials, including the prediction of atomic-level structures and bonding.[51] More specifically, the AIRSS method was expanded to electride research very recently. For example, in 2022, new structures of elemental sulfur with electride features were predicted under high pressures.[52] To further validate the reliability of the AIRSS method in predicting electride structures, we conducted validating calculations on a known electride system, namely $[(Li^+)_4N^{3-}\cdot e^-]$,[53] which exhibits many phases that are similar in energy, with 23 structures reported in the literature. Our calculations replicate the reported Li_4N structures, and we are therefore confident of the calculated structure of **1**.[46] A relatively short AIRSS search of 300 structures did not find the same lowest-energy structure reported in the literature[53] but did produce a structure only very slightly higher in energy (by 2.4 meV/atom), which contains the same characteristic NLi_8 polyhedra. Notably, although AIRSS finds structures that share motifs similar to those reported in the literature, it produces distinct phases not found in the literature,[53] which are nevertheless competitive in energy (within ~10 meV/atom), further highlighting the rich structural diversity in Li_4N. Therefore, we are confident that the calculated structure of **1** is reasonable.[46]

Interestingly, the AIRSS calculation of **1** suggests an unprecedented three-dimensional (3D) helical topology for the delocalized anionic electron density (Figure 2B). Anionic electrons can be visualized by taking the partial charge density of electrons just below the Fermi level[54]; we took the 12 electrons nearest to the Fermi level corresponding to the electrons donated by the 12 K atoms, which then become K^+ ions in the unit cell. In order to further confirm the electride nature of **1**, we calculated the

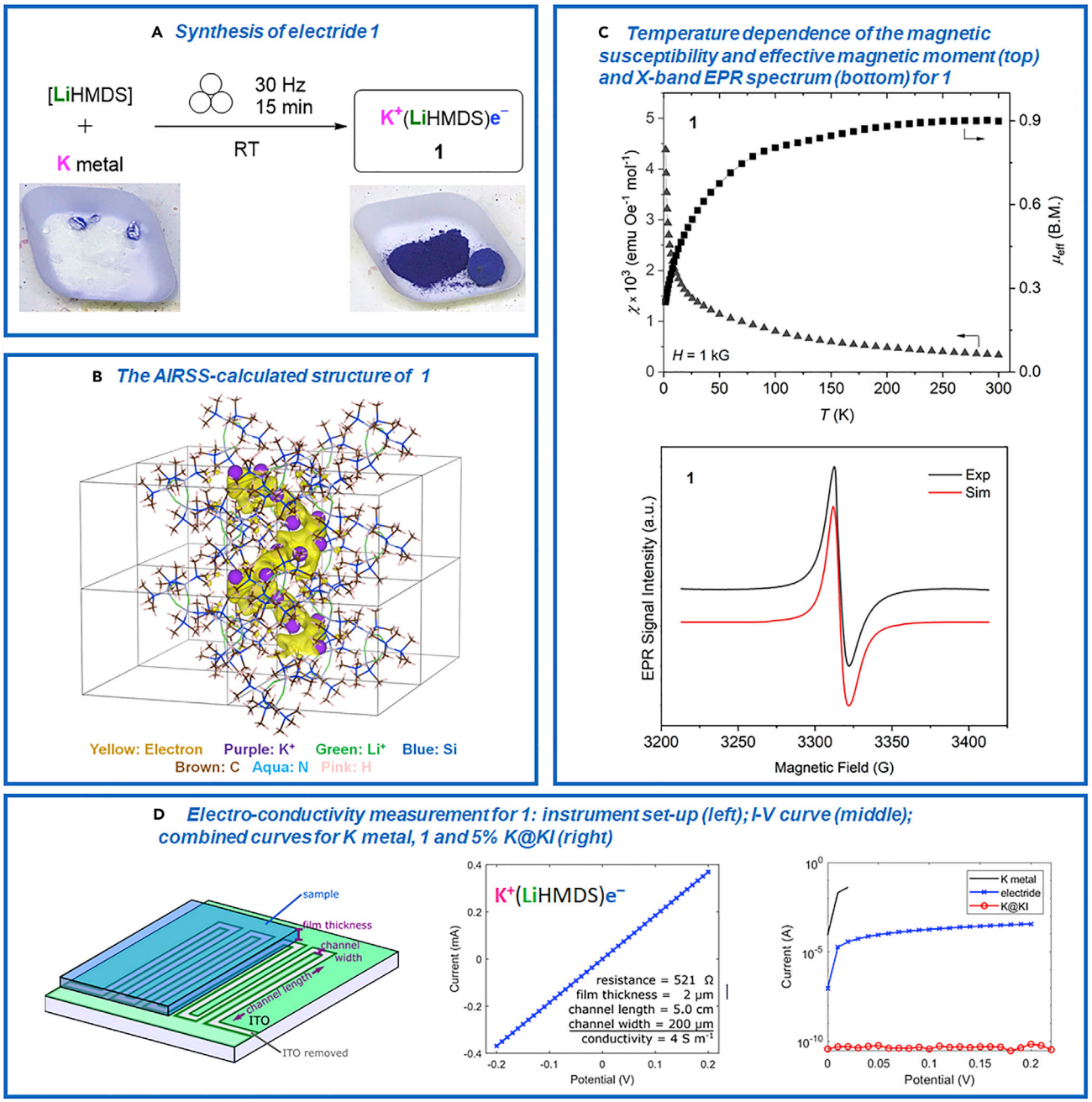

Figure 2. Synthesis and characterization of the electride K+(LiHMDS)e− (1)

(A) Mechanochemical ball milling synthesis of **1**.

(B) The calculated structure of **1**, with the helical anionic electron density topology highlighted in yellow.

(C) SQUID magnetometry at variable temperatures (top) and X-band EPR spectrum at 70 K (bottom, black) and its simulated version (bottom, red) for **1** (g_1 = 2.0013, g_2 = 2.0009, g_3 = 1.9951; linewidth ΔB_1 = 7.2 G, ΔB_2 = 7.2 G, ΔB_3 = 10.8 G).

(D) The electroconductivity measurements setup (left), the linear current (mA) versus potential (V) plot of **1** for calculating its electroconductivity (middle), and the current (A) versus potential (V) plots for K metal (black), **1** (blue), and 5% K@KI (red) (right).

electron localization function (ELF) and determined the locations of non-nuclear peaks that were not associated with covalent bonds in the LiHMDS (Figure S29B). We found that peaks occur in the interstitial spaces between groups of K^+ ions. Bader's quantum theory of atoms in molecules (QTAIM)[55] can be used to quantify

anionic electrons,[56] and we calculated an average charge of −0.73 for the basins associated with the interstitial sites identified in the model for **1**. Full details of these calculations can be found in the supplemental information. The anionic electron-confinement topologies play underpinning roles in electrides, determining their physicochemical properties. So far, zero-, one-, and two-dimensional (0D, 1D, and 2D) electrides have been well documented; their anionic electrons are confined to discrete cavities (0D), linear channels (1D), or planes (2D).[36] However, 3D electrides are far less examined other than a few *in silico* studies[53,57] and a six-electron hexagonal electride reported in 1994, which is unstable at room temperature.[58] Room-temperature-stable, scalable, and "bottleable" 3D electrides are highly desirable for their intriguing, and largely unpredictable, physicochemical properties. Although we are confident about the 3D helical anionic electron topology in **1**, supported by the AIRSS calculations and experimental magnetic data and electron paramagnetic resonance (EPR) spectroscopy (*vide infra*), we point out that several other structures were found in the AIRSS calculation to be close in energy (within 0.05 eV per formula unit), so there could be more than one phase present in **1**. Therefore, any specific details of the theoretical analysis may not be generally applicable across all phases that occur in **1**, but they nevertheless provide reassurance of the electride nature of the computational model of **1**. The predicted, lowest energy structure of **1** calculated at 0 K exhibits a metallic band structure (Figure S29A), which is corroborated by its electroconductivity measurement (*vide infra*), and it is non-magnetic. As the energy differences between this non-magnetic state and states in which the angular momenta of the electron spins no longer perfectly cancel are very small, calculations predict that **1** could be magnetic at finite temperatures, which we experimentally demonstrate below.

To experimentally confirm the presence of the anionic electrons, i.e., the "true electride" nature of **1**, we first measured its EPR spectrum. By definition, the anionic electrons in an electride do not bind to any nucleus, hence its EPR spectrum should exhibit signal(s) with no hyperfine coupling with spin-active nucleus (e.g., ^{1}H, ^{7}Li, ^{39}K, and ^{14}N). Such EPR criterion was recently employed by Martin and co-workers as crucial evidence to support their magnesium electride,[44] as well as in the $[Ca_{24}Al_{28}O_{64}]^{4+}4e^{-}$ inorganic electride of Hosono and co-workers.[40] Solid-state X-band EPR spectroscopy of **1** (Figure 2C, bottom, black) exhibits an asymmetric single-line spectrum at $g \sim 2$, with a peak-to-peak linewidth that varies from 38 G at room temperature to ca. 8.5 G at 5 K, and with no evidence of any hyperfine coupling due to ^{7}Li, ^{39}K, or ^{14}N nuclei. By definition, this fully and decisively supports the electride nature of **1**, proving that the electrons are not located on any of the Li^{+}, K^{+}, or $HMDS^{-}$ fragments, i.e., they exist as free anionic electrons. A simulation of the EPR spectrum at 70 K provided $g_1 = 2.0013$, $g_2 = 2.0009$, and $g_3 = 1.9951$ (Figure 2C, bottom, red).

Given that the EPR study confirmed that **1** is a genuine electride, we were curious to explore its physical properties, such as electroconductivity. Electrides were reported to exhibit versatile electroconductivity features[37] ranging from metal-like conductors (e.g., the classic 0D electride $[Ca_{24}Al_{28}O_{64}]^{4+}4e^{-}$)[40] to Mott insulators[59] (e.g., Sr_5P_3 and Yb_5Sb_3).[60,61] Given the 3D electron topology of **1**, it is intriguing to explore its electroconductivity. The electroconductivity of **1** was measured at 4 S m^{-1} by a finger-pattern method,[62] which is in the regime of conductor. For comparison, we also measured the electroconductivities of K metal (a conductive metal) and highly dispersed K metal over potassium iodide (5% K@KI)[63] (an insulator) (Figure 2D).

Beside the EPR and electroconductivity measurements, the anionic electrons in electrides have been reported to result in intriguing and usually complicated magnetic

properties.[40,64–68] The results of variable-temperature (2–300 K) magnetic susceptibility (χ) (Figure 2C) and variable-field (−7 to 7 T) magnetization (M) measurements (Figure S4), obtained with a superconducting quantum interference device (SQUID) magnetometer, confirmed the presence of unpaired electrons in **1**. The magnetic moment per $K^+(LiHMDS)e^-$ unit varies from 0.74 Bohr magneton (μ_B) at 300 K to 0.25 μ_B at 2 K (0.5 T applied field) (Figure 2C, top), suggesting dominant antiferromagnetic interactions between electrons. Closer examination of the magnetic data reveals fairly complex behavior, with multiple (at least two) magnetic interactions of different strengths operating in competition, in full agreement with the 3D helical nature of the delocalized free electrons. This evidence includes the following: (1) two regions of fit to a Curie-Weiss law above 60 K in the χ^{-1} versus T graph (Figure S2, red lines); (2) inflection in μ_{eff} versus T (Figure 2C, top); (3) irreversibility in zero-field cooled/field cooled (ZFC/FC) magnetization (Figure S3), indicating some sort of long-range ordering below 6 K[69]; and (4) small hysteresis loop at 2 K, which is asymmetric (M = 0 at H = −460 and +393 G) and persists more weakly at 4 K (Figure S5). The description as a 3D helical electride would be qualitatively consistent with nearest-neighbor, next-nearest-neighbor, and helical turn-to-turn magnetic interactions, which follow from the ideas used for topologically simpler electrides.[35–37] More detailed studies by complementary magnetic measurements and subsequent development of a model to explain this novel magnetic structure are awaited. Last but not least, before moving on to the reactivity studies of electride **1**, we would like to bring to our readers' attention that although the single-crystal structure of **1** has not yet been obtained and is likely to be amorphous, we believe that the presence of anionic electrons in **1** has been plausibly characterized by the abovementioned experiments and calculations. Electrides, by definition, do not necessarily link to crystalline phases as long as there are anionic electrons. For example, solvated electrons in liquid ammonia are treated as an electride phase but are not crystalline.[47,48]

Electride reactivity part 1: Benzene and pyridine C–H activation and C–C coupling

Given that electride **1** can be synthesized at 20 mmol scale[46] and is room-temperature stable under Ar or N_2 atmosphere, it could act as a user-friendly reagent in organic synthesis. Indeed, **1** reacted with benzene to produce a black solution, along with a small amount of solids and metal plates (Li or K). From the solution, we isolated sequentially black and colorless crystals by fractional crystallization. The structure of the black crystals was determined by single-crystal X-ray diffraction (SCXRD) to be a highly unusual lithium-potassium inverted-sandwich biphenyl complex $\{[(Li)(K)_2(\mu\text{-HMDS})_2]_2[\mu\text{-}\eta^{12}\text{-}(C_{12}H_{10})]\}$ (**2**) (Figures 3A and S18). The colorless crystals are a polymeric bridging heterobimetallic amide $[Li(\mu\text{-HMDS})K(\mu\text{-HMDS})]_\infty$ (**3**) (Figure S19). Considering the complexity of this reaction, the moderate but reproducible yields of **2** and **3** (28% for **2** and 12% for **3**) are satisfactory. From a synthetic chemistry perspective, the formation of **2** is remarkable because it is the first *reductive* tandem benzene C–H activation and C–C coupling, in sharp contrast with the well-documented *oxidative* processes,[7–12] which require precious-metal catalysts and/or hazardous strong oxidants. Although a comprehensive reaction pathway analysis is not feasible because of the unpaired electrons, density functional theory (DFT) calculations suggest a *bis*-cyclohexadienyl intermediate (A, Figure 3A) is plausible, indicating a mechanism in which the C–C bond formation occurs prior to the C–H cleavage (Figures S28 and S29), most likely via a de-aromatized cyclohexadienyl radical, and is followed by C–H activation and re-aromatization.

Complex **2** features a rare biphenyl dianion $[Bph]^{2-}$, which has only three unequivocally characterized precedents: a yttrium(III) complex $\{[(P_2N_2)Y(III)]_2[\mu\text{-}\eta^5\text{-}(C_{12}H_{10})]\}$

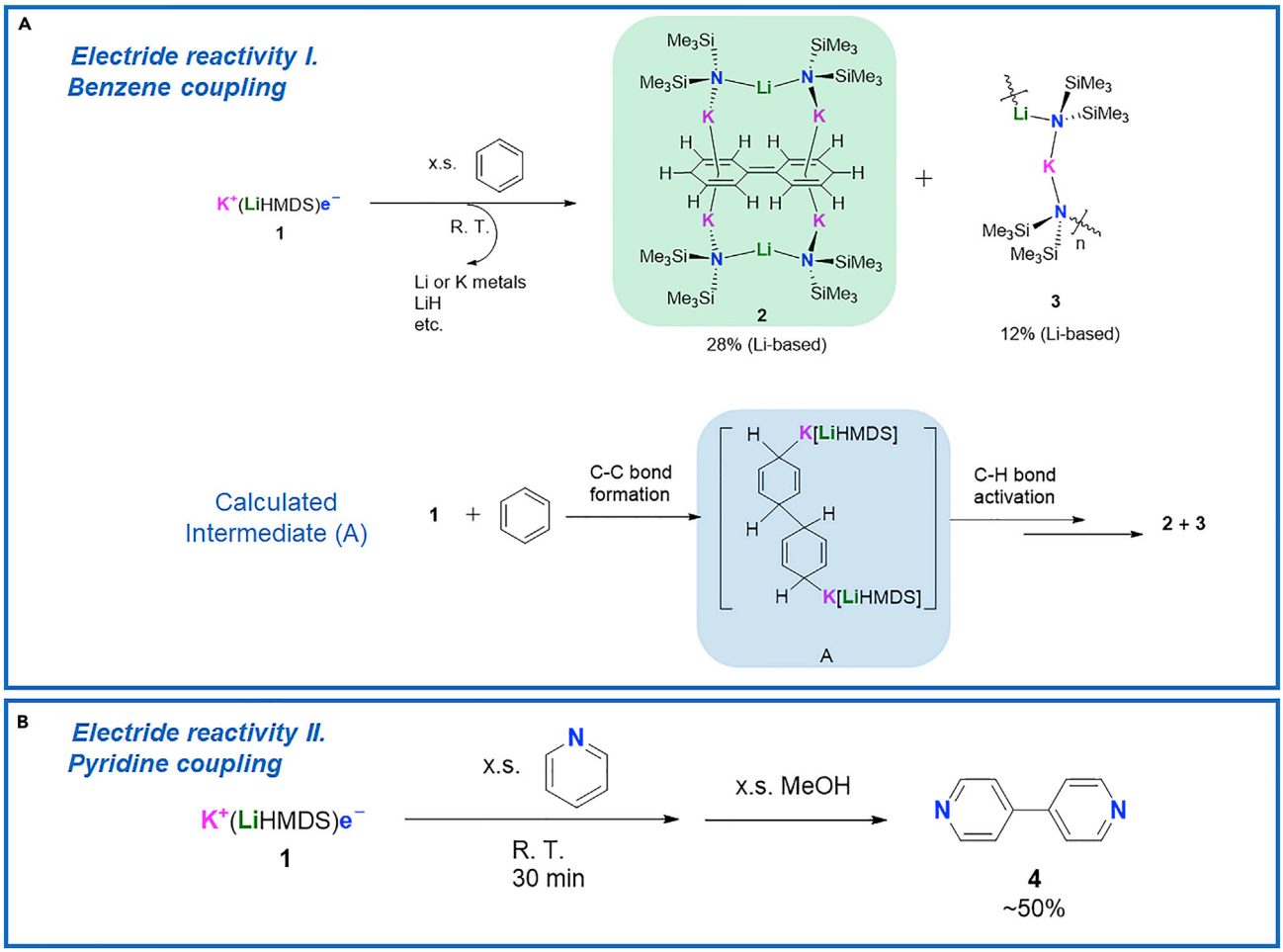

Figure 3. Electride reactivity part 1

Reductive C–H activation and C–C coupling of benzene (A) and pyridine (B) mediated by electride **1**. For single-crystal X-ray diffraction (SCXRD) structures of **2** and **3**, see Figures S18 and S19, respectively.

(P_2N_2 = $PhP(CH_2SiMe_2NSiMe_2CH_2)_2PPh$)[13] and two isostructural samarium(II) and ytterbium(II) complexes $\{[(NN^{TBS})RE(II)K]_2[\mu\text{-}\eta^6\text{-}RE\text{-}\eta^6\text{-}K\text{-}(C_{12}H_{10})]\}$ (RE = Sm, Yb; NN^{TBS} = $fc(NSi^tBuMe_2)_2$).[70] On the other hand, the Pt(II) alkyl-mediated benzene C–H activation and C–C coupling,[14] which are mentioned in the introduction, formed a heavily puckered phenyl-substituted dianionic cyclohexadienyl complex. The SCXRD structure of **2** (schematic presentation in Figure 3A; 50% thermal ellipsoids ORTEP [Oak Ridge Thermal-Ellipsoid Plot Program] presentation in Figure S18) exhibits alternating C=C double bonds (<1.40 Å) and C–C single bonds (>1.42 Å) in the biphenyl dianion, which were also observed in the SCXRD structures of the Y(III), Yb(II), and Sm(II) biphenyl dianionic complexes.[13,70] The most diagnostic structural parameter for the planarity of the biphenyl unit in **2** is the C^{ipso}–C^{ipso} (C1–C1^i) bond length of 1.395(3) Å, which is a typical C=C double bond. The 12 carbon atoms in the biphenyl dianion in **2** are all co-planar. These structural parameters suggest that the biphenyl dianion ($[Bph]^{2-}$) in **2** adopts a quinone-like structure (Figure 3A).

We employed DFT calculations to further understand the structure of **2**. The DFT calculations suggest that the highest occupied molecular orbital (HOMO) and the lowest unoccupied molecular orbital (LUMO) both locate on the biphenyl

fragment (Figure S32). As $[Bph]^{2-}$ could adopt singlet or triplet electronic states, we conducted spin density calculations to understand the electronic state of the $[Bph]^{2-}$ species in **2**. These concluded that **2** has a non-magnetic singlet ground state, implying all electrons in $[Bph]^{2-}$ are paired. Its lowest excited state is a triplet state, sitting at 9.9 kcal mol^{-1} above the singlet state (Figure S32). The non-magnetic ground state of the compound was confirmed by magnetic and EPR studies on several crystals, which both suggested that **2** has no unpaired electrons. However, there is a striking difference between the single-crystal and powder samples of **2** regarding their magnetic and EPR spectra. Finely ground powder sample of **2** become paramagnetic (Figure S17), while traces of monoanionic biphenyl radical are noticeable in the baseline of the EPR spectrum of single crystals of **2** (Figures S14 and S15). Specifically, while the single crystals of **2** are EPR silent, which matches its non-magnetic ground state, the ground powder sample of **2** exhibits an intense EPR signal with a one-line pattern and a linewidth of 1.3–1.8 G, resembling that of lithium metal.[71] We suspect that the biphenyl moiety in **2** is electronically labile, facilitating internal electron transfer[72–74] and even decomposition through crystal grinding. The formation of lithium metal, probably in the form of nanoparticles, could be rationalized by a redox couple Li(I) + $[Bph]^{2-}$ → Li(0) + $[Bph]^{1-\bullet}$. The result is surprising but not unexpected, particularly given that the biphenyl ligand is known for its facile $[Bph]^{0}$ ↔ $[Bph]^{1-\bullet}$ ↔ $[Bph]^{2-}$ disproportionation in reported group 1 metal biphenyl complexes.[75,76]

This biphenyl disproportionation may present challenges when interpreting the solution-state spectroscopic data of **2**, such as NMR and ultraviolet-visible (UV-vis) electronic absorption (*vide infra*), because the resultant monoanion radical $[Bph]^{1-\bullet}$ is paramagnetic and has strong absorption in the UV-vis region. Complex **2** is soluble in aromatic solvents (benzene and toluene) and partially soluble in aliphatic and ethereal solvents (hexane, THF, and Et_2O), forming black solutions. Its UV-vis spectrum in benzene (Figure S13) is dominated by a strong absorption band (λ_{max}) at circa 440 nm, with no significant absorption in the region of 500–600 nm, consistent with a $[Bph]^{2-}$ species.[75] A small shoulder at circa 410 nm could be assigned to a small percentage of the $[Bph]^{1-\bullet}$ radical. The concentration of this species is rather small, given that its characteristic strong absorption at 644 nm is hardly noticeable.[75,76] Therefore, we are confident that $[Bph]^{2-}$ is still the dominating biphenyl species of **2** in its benzene solution, i.e., the solid-state electronic structure of **2** is largely retained. Further evidence for the small disproportionation of biphenyl is obtained from solution-state NMR. The ^{1}H NMR spectrum of **2** in C_6D_6 (Figure S10) exhibits broad signals, whereas the ^{13}C NMR spectrum of **2** is largely featureless other than a weak signal of the methyl ($-CH_3$) groups of HMDS (Figure S11), despite a high solution concentration and long data acquisition time. In the ^{1}H NMR spectrum of **2** (Figure S10), three broad signals appear at 5.6, 4.2, and 3.5 ppm, which we assign to the $[Bph]^{2-}$ fragment, similarly to the diamagnetic Yb(II)/Y(III) $[Bph]^{2-}$ complexes.[13,70] We note that the ^{1}H integrals of these $[Bph]^{2-}$ signals are lower than expected (65%–75% of the expected ^{1}H integrals with the signal of the –HMDS group as a reference), supporting the hypothesis that a portion of the biphenyl is present in its paramagnetic monoanionic radical form. The neutral $[Bph]^{0}$ species, though, was not observed in the ^{1}H NMR spectrum (Figure S10). Indeed, the ^{7}Li NMR spectrum of **2** (Figure S12) exhibits two signals (3.03 and 1.70 ppm) despite repetitive recrystallization of the sample. The smaller ^{7}Li NMR signal at 3.03 ppm is in correspondence with a shoulder of the –HMDS signal in the ^{1}H NMR spectrum (Figure S10). This persisting presence of two sets of signals in the ^{7}Li and ^{1}H NMR spectra of **2**, along with its largely featureless ^{13}C NMR spectrum, supports the presence of paramagnetic $[Bph]^{1-\bullet}$ species, in agreement with the UV-vis and EPR data.

We attempted to treat **2** with mild oxidants (air and silver(I) iodide), proton sources (water and methanol) or electrophiles (Me_3SiCl and MeI), hoping to isolate biphenyl (Ph-Ph) or functionalized biphenyl. However, all of these attempts were unsuccessful: intractable mixtures of organic volatiles were produced, indicating the fragmentation of the biphenyl C–C bonds. Analyzing an aliquot of the methanol-quenched crude product suggested intractable mixtures with no presence of cyclohexadienes, indicating that the dianionic biphenyl complex **2** cannot be converted into the Birch reduction products (*vide infra*). On the other hand, to our gratification, reaction between **1** and an excess amount of pyridine produced 4,4′-bipyridine in 53% yield (assuming a stoichiometric **1**/pyridine ratio of 2:1) upon quenching with methanol (Figure 3B). C–H activation and C–C coupling of unactivated pyridine are challenging tasks. The most classical approaches for synthesizing the bipyridines involve reductive homocoupling of halogenated pyridines catalyzed by Cu, Ni, or Pd catalysts.[18] Specifically, most modern syntheses of 4,4′-bipyridine have to employ functionalized pyridines (such as halogen-pyridines, pyridyl boronic acids, or pyridyl sulfonic acids).[18] However, Anderson reported the very first 4,4′-bipyridine synthesis in 1868 by treating pyridine with sodium metal,[17] which obviously involves single-electron transfer (SET) processes and is distinct from the modern transition-metal catalyzed cross-coupling approach.[18] As a result of the unamiable sodium metal condition, the SET approach toward 4,4′-bipyridine has been largely overlooked. Our result herein suggests that facile and transition-metal-free reductive coupling of pyridine is a viable route for constructing bipyridines. Expanding the substrate scope into substituted pyridines is underway, but it is beyond the scope of this work and will be presented separately in due course.

Electride reactivity part 2: Solvent-free Birch reductions

Encouraged by the benzene and pyridine reactions, we studied the reactivity of **1** toward more aromatic organic substrates. At this early stage of research, ten substrates were studied as a proof of concept: (1) six hydrocarbon arenes with different substituents (**5a**–**5f**), (2) two *N*-hetero-arenes (**5g** and **5h**), and (3) two aryl carboxylic acids (**5i** and **5j**) (Figure 4). We would like to emphasize that although the substrate scope is not comprehensive, as a proof of concept, we cover arenes and hetero-arenes with electron-donating and electron-withdrawing groups. Moreover, we include two aryl carboxylic acids, which are of significant interest in organic synthesis.

Treating the substrates (**5a**–**5e** and **5h**–**5j**) with 2.2–3.0 equiv of **1** under mechanochemical ball mill conditions for 20–25 min produced intensely colored, highly air-sensitive solids. After quenching with excess of degassed methanol under Ar and the subsequent standard organic chemistry workup,[46] corresponding Birch reduction products (**6a**–**6e** and **6h**–**6j**) were obtained in good to excellent yields (58%–96%) (Figure 4), representing the first solvent-free Birch-type reductions. Compared with the previous dissolved metal, electrochemical, and photochemical methods, electride reagent **1** exhibits intriguing differences regarding regio- and chemo-selectivities. For example, the acridine (**5h**) was reduced in 80% yield herein, whereas a recently reported photochemical Birch reduction achieved a moderate 43% yield.[28] Moreover, the prevailing over-reduction of naphthalene (**5a**), i.e., reduction occurs at both of the phenyl rings, was not observed in our case: **6a** was isolated as the only product. For six out of eight cases (**6a**–**6d**, **6h**, and **6i**), only one product was isolated, and no column chromatograph was needed for purifications. For the reductions of **5e** and **5j**, the selectivities are less optimized, but there is still only one major product (**6e** and **6j**, respectively), too. Here, we would like to focus our readers' attention on the role of electride **1** in the Birch reductions. By definition, a stoichiometric electron source (i.e., electron donor) is essential for Birch

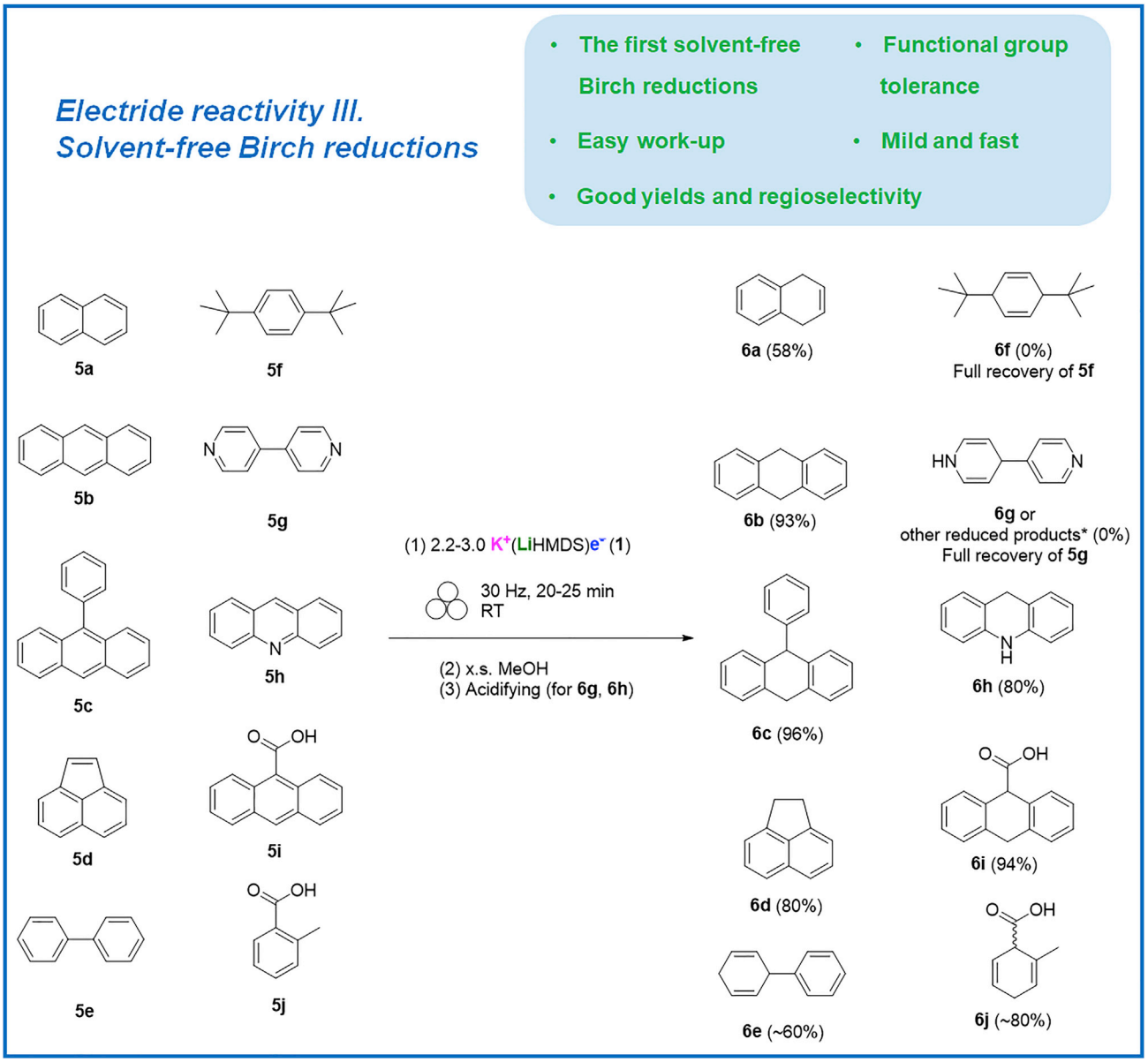

Figure 4. Electride reactivity part 2

Solvent-free Birch reductions mediated by electride **1**.

*The reduction of 4,4′-bipyridine (**5g**) could produce more than one product, such as **6g**, 1,1′,4,4′-tetrahydro-4,4′-bipyridine, 1*H*,1′*H*-4,4′-bipyridinylidene, or bipyridinyl anion radical; see Formanuik et al.[77] and Carrington and dos Santos-Veiga[78] for examples. In our case, however, none of the products were observed instead of a full recovery of **5g**.

reduction. The electron donor could be chemical (e.g., Na-NH_3(l)), electrochemical (electricity), or photochemical (e.g., OH^- of NH_4OH[27] and diisopropylethyl amine[28]). In our Birch reduction cases, electride **1** acts as a solvent-free, catalyst-free, facile electron donor. The role of electride **1** herein should not be confused with the electride-catalyzed reactions, e.g., the topical N_2-to-NH_3 reaction ($N_2 + 3H_2 \rightarrow 2NH_3$),[79,80] which, thermodynamically speaking, does not involve net electron input. Despite being described as an electron donor,[80] the role of electrides in the N_2 activation is shuttling electrons between H_2 (the ultimate stoichiometric electron source) and N_2.

Despite working well with the **5a–5e** and **5h–5j**, the attempt to reduce the electron-rich 1,4-*di*-tert-butylbenzene (**5f**) was not successful and led to a full recovery of the starting material. This is probably because the two electron-donating *tert*-butyls quench the initial nucleophilic de-aromatization attack by the anionic electrons in **1**. This hypothesis was corroborated by observing the reaction mixture of **5f** and **1**, where no color change was observed after ball milling before quenching (a mixture of white [**5f**] and blue [**1**] solids). This is in stark contrast with the intensely colored intermediates for **5a–5e** (black to purple solids), which we hypothesized to be radical species. In the case of **5f**, the radical species did not form, due to the hampered initial electron transfer and de-aromatization. However, this hypothesis does not work in the case of **5g**, which does indeed produce a deep-purple intermediate. But after quenching, only the starting material **5g** was recovered. The case of **5g** is particularly interesting in comparison with **5e**, where the Birch reduction product **6e** was observed as the major product. We attribute the recovery of **5g** to a base-promoted deprotonation and re-aromatization after quenching, which was initiated by deprotonation of the –NH (a Brønsted acid) of **6g** by the abundant lithium/potassium methoxide and LiHMDS in the system (Brønsted bases), followed by air oxidation and re-aromatization, to reproduce **5g**. Similar deprotonation aromatization of 1,4-dihydro-4,4′-bipyridines under basic and oxidative (air and/or oxidants) conditions in aqueous phase was reported.[81,82]

Beside the solvent-free condition, another noteworthy difference between our electride-mediated Birch reductions and all the previous methods is that in our cases, the reactions were conducted under aprotic conditions until the quenching stage, i.e., our method does not need *in situ* proton sources before the quenching stage. This is in stark contrast to previous reports, which all show that *in situ* proton sources, and in some cases hydrogen atom transfer (HAT) reagents, are required.[28] The necessity of the *in situ* H^+ or $H^\bullet$ in these previous reports is in coherence with the widely accepted stepwise mechanism scenario, where H^+ or $H^\bullet$ is needed to convert the initially formed radical anion into a carbanion.[83] The absence of the *in situ* H^+ and $H^\bullet$ source in our cases, on the other hand, may indicate a significantly different mechanism. However, it is difficult to experimentally monitor our mechanochemical reactions, given the fact that they took place in the solid state in vigorously moving reaction jars. Meanwhile, quantum chemical calculations to probe the Birch reduction mechanism are challenging (large because of the open-shell nature of the system); hence, the Birch reduction mechanism is still far from well understood. Although beyond the scope of this paper, we are developing comprehensive experimental and theoretical approaches to elucidate the in-depth mechanism of our solid-state electride-mediated solvent-free Birch reductions, and the results will be reported in due course.

Conclusions and outlook

In conclusion, we report a facile and scalable mechanochemical synthesis of the RoSE K^+(LiHMDS)e^- (**1**), which features an unprecedented 3D helical electron confinement topology, leading to unique physical properties such as in magnetism. Moreover, **1** is a versatile reagent in organic synthesis, mediating the facile transition-metal-free benzene and pyridine C–H activation and C–C coupling, and the first solvent-free Birch-type reductions. Further work is underway in three directions: (1) expanding the organic reaction substrate scopes and exploring applications of our method in late-stage functionalization of complicated pharmaceutical molecules; (2) exploring the usage of **1** in other organic reactions, especially the SET reactions; and (3) expanding this group 1 heterometallic electride family and thoroughly

understanding their physicochemical properties, as well as exploring their applications in materials science.

EXPERIMENTAL PROCEDURES

Resource availability

Lead contact

Further information and requests for resources and materials should be directed to and will be fulfilled by the lead contact, Dr. Erli Lu (erli.lu@newcastle.ac.uk).

Materials availability

This study did not generate new materials.

Data and code availability

This study did not generate new code. The experimental and computational methods, as well as characterization data of new compounds, are available in the supplemental information. The supplemental crystallographic data for complexes **2** and **3** are available under CCDC: 2166312 and 2166313, respectively. These data can be obtained free of charge from the Cambridge Crystallographic Data Centre (12 Union Road, Cambridge CB2 1EZ, UK) via web (https://www.ccdc.cam.ac.uk/structures/), email (data_request@ccdc.cam.ac.uk), or fax (+44 1223 336033).

SUPPLEMENTAL INFORMATION

Supplemental information can be found online at https://doi.org/10.1016/j.chempr.2022.11.006.

ACKNOWLEDGMENTS

The authors thank the Newcastle University Chemistry Technical Support Team (Dr. Laura McCorkindale, Dr. Amy Roberts, and Mr. Niall Straughan) for supporting their research. E.L. thanks Drs. Roly Armstrong and Keith Izod, as well as Profs. Michael Waring and Bernard Golding (all at Newcastle University), for their insightful discussions. E.L., J.A.D., and M.F. thank the Newcastle University Academic Track (NUAcT) Fellowship Scheme for financial support. N.D. thanks Newcastle University for a NUAcT PhD studentship. J.A.D. gratefully acknowledges the EPSRC (EP/V013130/1) for funding; via membership of the UK's HEC Materials Chemistry Consortium, which is funded by the EPSRC (EP/R029431), this work used the ARCHER2 UK National Supercomputing Service. E.L. thanks the EPSRC North East Centre of Energy Materials (NECEM) and the Royal Society of Chemistry Research Enablement Grant (E20-5153) for financial support to build the mechanochemistry facility. The authors thank the EPSRC National Research Facility for EPR Spectroscopy (NS/A000055/1) for EPR and magnetometry measurements. C.L.M. thanks the University of Bath for access to the Anatra and Balena High Performance Computing Services. This work is dedicated to the memory of Prof. James L. Dye (Michigan State University; 1927–2021), a pioneer in electride chemistry.

AUTHOR CONTRIBUTIONS

N.D. and E.L. conceptualized the central idea and designed and conducted the syntheses and characterization. J.A.Q. and J.A.D. designed and conducted the AIRSS calculations for **1**. F.T. and D.C. collected and analyzed the EPR and SQUID magnetometry data. C.L.M. designed and conducted the molecular geometries and the orbital and reaction intermediate calculations for **2**. H.M., G.H.M., and M.F. collected and analyzed the electroconductivity data. P.G.W. and J.A.G. collected and analyzed the single-crystal and powder X-ray diffraction data, respectively.

E.L. supervised the work, analyzed the data, and wrote the manuscript with contributions from all the authors.

DECLARATION OF INTERESTS

The authors declare no competing interests.

INCLUSION AND DIVERSITY

We support inclusive, diverse, and equitable conduct of research.

Received: August 4, 2022
Revised: October 4, 2022
Accepted: November 6, 2022
Published: December 1, 2022

REFERENCES

1. Protti, S., and Palmieri, A. (2021). Sustainable Organic Synthesis: Tools and Strategies (the Royal Society of Chemistry). https://doi.org/10.1039/9781839164842.

2. Kekulé, A. (1872). Ueber einige Condensationsproducte des Aldehyds. Ann. Chem. Pharm. *162*, 77–124. https://doi.org/10.1002/jlac.18721620110.

3. Friedel, C., and Crafts, J.M. (1877). Sur Une nouvelle méthode générale de synthèse d'hydrocarbures, d'acétones, etc. Compt. Rend. *84*, 1392–1395.

4. Birch, A.J. (1944). 117. Reduction by dissolving metals. Part I. J. Chem. Soc. 430–436. https://doi.org/10.1039/JR9440000430.

5. Sandmeyer, T. (1884). Ueber die ersetzung der amidgruppe durch chlor in den aromatischen substanzen. Ber. Dtsch. Chem. Ges. *17*, 1633–1635. https://doi.org/10.1002/cber.18840170219.

6. Scholl, R., and Mansfeld, J. (1910). *meso*-Benzdianthron (helianthron), *meso*-naphthodianthron, und ein neuer weg zum flavanthren. Ber. Dtsch. Chem. Ges. *43*, 1734–1746. https://doi.org/10.1002/cber.19100430288.

7. Grzybowski, M., Skonieczny, K., Butenschön, H., and Gryko, D.T. (2013). Comparison of oxidative aromatic coupling and the Scholl reaction. Angew. Chem. Int. Ed. *52*, 9900–9930. https://doi.org/10.1002/anie.201210238.

8. Yoshimura, A., and Zhdankin, V.V. (2016). Advances in synthetic applications of hypervalent iodine compounds. Chem. Rev. *116*, 3328–3435. https://doi.org/10.1021/acs.chemrev.5b00547.

9. Ashenhurst, J.A. (2010). Intermolecular oxidative cross-coupling of arenes. Chem. Soc. Rev. *39*, 540–548. https://doi.org/10.1039/B907809F.

10. Lv, F., and Yao, Z.-J. (2017). Recent advances in direct dehydrogenative biphenyl couplings. Sci. China Chem. *60*, 701–720. https://doi.org/10.1007/s11426-016-0435-5.

11. Yeung, C.S., and Dong, V.M. (2011). Catalytic dehydrogenative cross-coupling: Forming carbon–carbon bonds by oxidizing two carbon–hydrogen bonds. Chem. Rev. *111*, 1215–1292. https://doi.org/10.1021/cr100280d.

12. Chen, X., Engle, K.M., Wang, D.H., and Yu, J.Q. (2009). Palladium(II)-catalyzed C–H activation/C–C cross-coupling reactions: Versatility and practicality. Angew. Chem. Int. Ed. *48*, 5094–5115. https://doi.org/10.1002/anie.200806273.

13. Fryzuk, M.D., Love, J.B., and Rettig, S.J. (1997). Arene coordination to yttrium(III) via carbon–carbon bond formation. J. Am. Chem. Soc. *119*, 9071–9072. https://doi.org/10.1021/ja9719743.

14. Konze, W.V., Scott, B.L., and Kubas, G.J. (2002). C–H activation and C–C coupling of arenes by cationic. J. Am. Chem. Soc. *124*, 12550–12556. https://doi.org/10.1021/ja020798h.

15. Brand, S., Elsen, H., Langer, J., Grams, S., and Harder, S. (2019). Calcium-catalyzed arene C–H bond activation by low-valent Al^{I}. Angew. Chem. Int. Ed. *58*, 15496–15503. https://doi.org/10.1002/anie.201908978.

16. Grams, S., Eyselein, J., Langer, J., Färber, C., and Harder, S. (2020). Boosting low-valent aluminum(I) reactivity with a potassium reagent. Angew. Chem. Int. Ed. *59*, 15982–15986. https://doi.org/10.1002/anie.202006693.

17. Anderson, T. (1868). On the products of the destructive distillation of animal substances. Part V. Trans. R. Soc. Edinb. *25*, 205–216.

18. Hapke, M., Brandt, L., and Lützen, A. (2008). Versatile tools in the construction of substituted 2,2′-bipyridines—Cross-coupling reactions with tin, zinc and boron compounds. Chem. Soc. Rev. *37*, 2782–2797. https://doi.org/10.1039/B810973G.

19. Parikh, A., Parikh, H., and Parikh, K. (2006). Chapter 18. Birch reduction. In Name Reactions in Organic Synthesis. (Foundation Books), pp. 69–72. https://doi.org/10.1017/UPO9788175968295.020.

20. Donohoe, T.J., Garg, R., and Stevenson, C.A. (1996). Prospects for stereo-control in the reduction of aromatic compounds. Tetrahedron Asymmetry *7*, 317–344. https://doi.org/10.1016/0957-4166(96)00001-8.

21. Rao, G.S.R.S. (2003). Birch reduction and its application in the total synthesis of natural products. Pure Appl. Chem. *75*, 1443–1451. https://doi.org/10.1351/pac200375101443.

22. Wertjes, W.C., Southgate, E.H., and Sarlah, D. (2018). Recent advances in chemical dearomatization of nonactivated arenes. Chem. Soc. Rev. *47*, 7996–8017. https://doi.org/10.1039/C8CS00389K.

23. Peters, B.K., Rodriguez, K.X., Reisberg, S.H., Beil, S.B., Hickey, D.P., Kawamata, Y., Collins, M., Starr, J., Chen, L., Udyavara, S., et al. (2019). Scalable and safe synthetic organic electroreduction inspired by Li-ion battery chemistry. Science *363*, 838–845. https://doi.org/10.1126/science.aav5606.

24. Tiwari, V.K., Powell, D.R., Broussy, S., and Berkowitz, D.B. (2021). Rapid enantioselective and diastereoconvergent hybrid organic/biocatalytic entry into the oseltamivir core. J. Org. Chem. *86*, 6494–6503. https://doi.org/10.1021/acs.joc.1c00326.

25. Hayashi, K., Griffin, J., Harper, K.C., Kawamata, Y., and Baran, P.S. (2022). Chemoselective (hetero) arene electroreduction enabled by rapid alternating polarity. J. Am. Chem. Soc. *144*, 5762–5768. https://doi.org/10.1021/jacs.2c02102.

26. Yoshimi, Y., Ishise, A., Oda, H., Moriguchi, Y., Kanezaki, H., Nakaya, Y., Katsuno, K., Itou, T., Inagaki, S., Morita, T., and Hatanaka, M. (2008). Hydroxide ion as electron source for photochemical Birch-type reduction and photodehalogenation. Tetrahedron Lett. *49*, 3400–3404. https://doi.org/10.1016/j.tetlet.2008.03.123.

27. Cole, J.P., Chen, D.F., Kudisch, M., Pearson, R.M., Lim, C.H., and Miyake, G.M. (2020). Organocatalyzed Birch reduction driven by visible light. J. Am. Chem. Soc. *142*, 13573–13581. https://doi.org/10.1021/jacs.0c05899.

28. Chatterjee, A., and König, B. (2019). Birch-type photoreduction of arenes and heteroarenes by sensitized electron transfer. Angew. Chem. Int. Ed. *58*, 14289–14294. https://doi.org/10.1002/anie.201905485.

29. Thiele, B., Rieder, O., Golding, B.T., Müller, M., and Boll, M. (2008). Mechanism of enzymatic Birch reduction: Stereochemical course and

exchange reactions of benzoyl-CoA reductase. J. Am. Chem. Soc. *130*, 14050–14051. https://doi.org/10.1021/ja805091w.

30. Donohoe, T.J., and House, D. (2002). Ammonia free partial reduction of aromatic compounds using lithium di-tert-butylbiphenyl (LiDBB). J. Org. Chem. *67*, 5015–5018. https://doi.org/10.1021/jo0257593.

31. Donohoe, T.J., Sintim, H.O., Sisangia, L., Ace, K.W., Guyo, P.M., Cowley, A., and Harling, J.D. (2005). Utility of the ammonia-free Birch reduction of electron-deficient pyrroles: Total synthesis of the 20S proteasome inhibitor, *clasto*-Lactacystin ß-lactone. Chem. Eur. J. *11*, 4227–4238. https://doi.org/10.1002/chem.200401119.

32. Donohoe, T.J., and Thomas, R.E. (2007). The partial reduction of electron-deficient pyrroles: Procedures describing both Birch (Li/NH_3) and ammonia-free (Li/DBB) conditions. Nat. Protoc. *2*, 1888–1895. https://doi.org/10.1038/nprot.2007.245.

33. Lei, P., Ding, Y., Zhang, X., Adijiang, A., Li, H., Ling, Y., and An, J. (2018). A practical and chemoselective ammonia-free Birch reduction. Org. Lett. *20*, 3439–3442. https://doi.org/10.1021/acs.orglett.8b00891.

34. Burrows, J., Kamo, S., and Koide, K. (2021). Scalable Birch reduction with lithium and ethylenediamine in tetrahydrofuran. Science *374*, 741–746. https://doi.org/10.1126/science.abk3099.

35. Dye, J.L. (2009). Electrides: Early examples of quantum confinement. Acc. Chem. Res. *42*, 1564–1572. https://doi.org/10.1021/ar9000857.

36. Liu, C., Nikolaev, S.A., Ren, W., and Burton, L.A. (2020). Electrides: A review. J. Mater. Chem. C *8*, 10551–10567. https://doi.org/10.1039/D0TC01165G.

37. Hosono, H., and Kitano, M. (2021). Advances in materials and applications of inorganic electrides. Chem. Rev. *121*, 3121–3185. https://doi.org/10.1021/acs.chemrev.0c01071.

38. Lee, K., Kim, S.W., Toda, Y., Matsuishi, S., and Hosono, H. (2013). Dicalcium nitride as a two-dimensional electride with an anionic electron layer. Nature *494*, 336–340. https://doi.org/10.1038/nature11812.

39. Yoo, B.I., Kim, Y.J., You, Y.M., Yang, J.W., and Kim, S.W. (2018). Birch reduction of aromatic compounds by inorganic electride $[Ca_2N]^{+}{\cdot}e^{-}$ in an alcoholic solvent: An analogue of solvated electrons. J. Org. Chem. *83*, 13847–13853. https://doi.org/10.1021/acs.joc.8b02094.

40. Matsuishi, S., Toda, Y., Miyakawa, M., Hayashi, K., Kamiya, T., Hirano, M., Tanaka, I., and Hosono, H. (2003). High-density electron anions in a nanoporous single crystal: $[Ca_{24}Al_{28}O_{64}]^{4+}(4e^{-})$. Science *301*, 626–629. https://doi.org/10.1126/science.1083842.

41. Mizoguchi, H., Park, S.W., Katase, T., Vazhenin, G.V., Kim, J., and Hosono, H. (2021). Origin of metallic nature of Na_3N. J. Am. Chem. Soc. *143*, 69–72. https://doi.org/10.1021/jacs.0c11047.

42. Li, K., Gong, Y.-T., Wang, J.-J., and Hosono, H. (2021). Electron-deficient-type electride Ca_5Pb_3: Extension of electride chemical space. J. Am. Chem. Soc. *143*, 8821–8828. https://doi.org/10.1021/jacs.1c03278.

43. Redko, M.Y., Jackson, J.E., Huang, R.H., and Dye, J.L. (2005). Design and synthesis of a thermally stable organic electride. J. Am. Chem. Soc. *127*, 12416–12422. https://doi.org/10.1021/ja053216f.

44. Day, C.S., Do, C.D., Odena, C., Benet-Buchholz, J., Xu, L., Foroutan-Nejad, C., Hopmann, K.H., and Martin, R. (2022). Room-temperature-stable magnesium electride via Ni(II) reduction. J. Am. Chem. Soc. *144*, 13109–13117. https://doi.org/10.1021/jacs.2c01807.

45. James, S.L., Adams, C.J., Bolm, C., Braga, D., Collier, P., Friščić, T., Grepioni, F., Harris, K.D.M., Hyett, G., Jones, W., et al. (2012). Mechanochemistry: Opportunities for new and cleaner synthesis. Chem. Soc. Rev. *41*, 413–447. https://doi.org/10.1039/C1CS15171A.

46. See the supplemental information for full experimental and computational details.

47. Edwards, P.P. (1982). The electronic properties of metal solutions in liquid ammonia and related solvents. Adv. Inorg. Chem. *25*, 135–185. https://doi.org/10.1016/S0898-8838(08)60140-3.

48. Buttersack, T., Mason, P.E., McMullen, R.S., Schewe, H.C., Martinek, T., Brezina, K., Crhan, M., Gomez, A., Hein, D., Wartner, G., et al. (2020). Photoelectron spectra of alkali metal–ammonia microjets: From blue electrolyte to bronze metal. Science *368*, 1086–1091. https://doi.org/10.1126/science.aaz7607.

49. Dye, J.L. (2003). Chemistry. Electrons as anions. Science *301*, 607–608. https://doi.org/10.1126/science.1088103.

50. Pickard, C.J., and Needs, R.J. (2011). Ab initio random structure searching. J. Phys. Condens. Matter *23*, 053201. https://doi.org/10.1088/0953-8984/23/5/053201.

51. Harper, A.F., Evans, M.L., Darby, J.P., Karasulu, B., Koçer, C.P., Nelson, J.R., and Morris, A.J. (2020). Ab initio structure prediction methods for battery materials a review of recent computational efforts to predict the atomic level structure and bonding in materials for rechargeable batteries. Johnson Matthey Technol. Rev. *64*, 103–118. https://doi.org/10.1595/205651320X15742491027978.

52. Whaley-Baldwin, J., and Pickard, C.J. (2022). Suppression of the superconducting phase in new structures of elemental sulfur at terapascal pressures. Phys. Rev. B *105*, 144105. https://doi.org/10.1103/PhysRevB.105.144105.

53. Tsuji, Y., Dasari, P.L.V.K., Elatresh, S.F., Hoffmann, R., and Ashcroft, N.W. (2016). Structural diversity and electron confinement in Li_4N: Potential for 0-D, 2-D, and 3-D electrides. J. Am. Chem. Soc. *138*, 14108–14120. https://doi.org/10.1021/jacs.6b09067.

54. Tsuji, Y., Hori, M., and Yoshizawa, K. (2020). Theoretical study on the electronic structure of heavy alkali-metal suboxides. Inorg. Chem. *59*, 1340–1354. https://doi.org/10.1021/acs.inorgchem.9b03046.

55. Bader, R.F.W. (1990). Atoms in Molecules: A Quantum Theory (Clarendon Press).

56. Tsuji, Y., Hashimoto, W., and Yoshizawa, K. (2019). Lithium-richest phase of lithium Tetrelides $Li_{17}Tt_4$ (Tt = Si, Ge, Sn, and Pb) as an electride. Bull. Chem. Soc. Jpn. *92*, 1154–1169. https://doi.org/10.1246/bcsj.20190040.

57. Zhang, Y., Wang, H., Wang, Y., Zhang, L., and Ma, Y. (2017). Computer-assisted inverse design of inorganic electrides. Phys. Rev. X *7*, 011017. https://doi.org/10.1103/PhysRevX.7.011017.

58. Wagner, M.J., Huang, R.H., Eglin, J.L., and Dye, J.L. (1994). An electride with a large six-electron ring. Nature *368*, 726–729. https://doi.org/10.1038/368726a0.

59. Mott, N.F., and Peierls, R. (1937). Discussion of the paper by de Boer and Verwey. Proc. Phys. Soc. *49*, 72–73. https://doi.org/10.1088/0959-5309/49/4S/308.

60. Wang, J.-J., Hanzawa, K., Hiramatsu, H., Kim, J., Umezawa, N., Iwanaka, K., Tada, T., and Hosono, H. (2017). Exploration of stable strontium phosphide-based electrides: Theoretical structure prediction and experimental validation. J. Am. Chem. Soc. *139*, 15668–15680. https://doi.org/10.1021/jacs.7b06279.

61. Lu, Y.-F., Wang, J.-J., Li, J., Wu, J.-Z., Kanno, S., Tada, T., and Hosono, H. (2018). Realization of Mott-insulating electrides in dimorphic Yb_5Sb_3. Phys. Rev. B *98*, 125128. https://doi.org/10.1103/PhysRevB.98.125128.

62. Morritt, G.H., Michaels, H., and Freitag, M. (2022). Coordination polymers for emerging molecular devices. Chem. Phys. Rev. *3*, 011306. https://doi.org/10.1063/5.0075283.

63. Hicks, J., Juckel, M., Paparo, A., Dange, D., and Jones, C. (2018). Multigram syntheses of magnesium(I) compounds using alkali metal halide supported alkali metals as dispersible reducing agents. Organometallics *37*, 4810–4813. https://doi.org/10.1021/acs.organomet.8b00803.

64. Park, J., Lee, K., Lee, S.Y., Nandadasa, C.N., Kim, S., Lee, K.H., Lee, Y.H., Hosono, H., Kim, S.G., and Kim, S.W. (2017). Strong localization of anionic electrons at interlayer for electrical and magnetic anisotropy in two-dimensional Y_2C electride. J. Am. Chem. Soc. *139*, 615–618. https://doi.org/10.1021/jacs.6b11950.

65. Hiraishi, M., Kojima, K.M., Yamauchi, I., Okabe, H., Takeshita, S., Koda, A., Kadono, R., Zhang, X., Matsuishi, S., Hosono, H., et al. (2018). Electronic correlation in the quasi-two-dimensional electride Y_2C. Phys. Rev. B *98*, 041104. https://doi.org/10.1103/PhysRevB.98.041104.

66. Lee, S.Y., Hwang, J.Y., Park, J., Nandadasa, C.N., Kim, Y., Bang, J., Lee, K., Lee, K.H., Zhang, Y., Ma, Y., et al. (2020). Ferromagnetic quasi-atomic electrons in two-dimensional electride. Nat. Commun. *11*, 1526. https://doi.org/10.1038/s41467-020-15253-5.

67. Meng, W., Zhang, X., Liu, Y., Dai, X., Gao, H., and Liu, G. (2021). Two-dimensional $[CaCl]^{+}{\cdot}e^{-}$ with its strippable feasibility as an applicable electride with room-temperature ferromagnetism and extremely low work function. J. Mater. Chem. C *9*, 15477–15487. https://doi.org/10.1039/D1TC04356K.

68. Novoselov, D.Y., Korotin, D.M., Shorikov, A.O., Anisimov, V.I., and Oganov, A.R. (2021). Interacting electrons in two-dimensional electride Ca_2N. J. Phys. Chem. C *125*, 15724–15729. https://doi.org/10.1021/acs.jpcc.1c04485.

69. Fust, S., Mukherjee, S., Paul, N., Stahn, J., Kreuzpaintner, W., Böni, P., and Paul, A. (2016). Realizing topological stability of magnetic helices in exchange-coupled multilayers for all-spin-based system. Sci. Rep. *6*, 33986. https://doi.org/10.1038/srep33986.

70. Xiao, Y., Zhao, X.K., Wu, T., Miller, J.T., Hu, H.S., Li, J., Huang, W., and Diaconescu, P.L. (2020). Distinct electronic structures and bonding interactions in inverse-sandwich samarium and ytterbium biphenyl complexes. Chem. Sci. *12*, 227–238. https://doi.org/10.1039/D0SC03555F.

71. Niemöller, A., Jakes, P., Eichel, R.A., and Granwehr, J. (2018). EPR imaging of metallic lithium and its application to dendrite localisation in battery separators. Sci. Rep. *8*, 14331. https://doi.org/10.1038/s41598-018-32112-y.

72. Noordik, J.H., Schreurs, J., Gould, R.O., Mooij, J.J., and De Boer, E. (1978). Molecular and magnetic structure of the paramagnetic ion pair bis (tetraglyme) potassium biphenyl. J. Phys. Chem. *82*, 1105–1110. https://doi.org/10.1021/j100499a003.

73. Mooij, J.J., Klaassen, A.A.K., De Boer, E., Degens, H.M.L., Van den Hark, T.E.M., and Noordik, J.H. (1976). Molecular and magnetic structure of the paramagnetic ion pair bis(tetraglyme)rubidium biphenyl, $Rb^+[CH_3O(CH_2CH_2O)_4CH_3]_2C_{12}H_{10}^-$. J. Am. Chem. Soc. *98*, 680–685. https://doi.org/10.1021/ja00419a008.

74. Canters, G.W., Klassen, A.A.K., and De Boer, E. (1970). Investigations on single crystals of alkali$^+$ biphenyl$^-$ radical salts. J. Phys. Chem. *74*, 3299–3302. https://doi.org/10.1021/j100711a029.

75. Bondarchuk, S.V., Carrera, M., de la Viuda, M., and Guijarro, A. (2018). Spontaneous disproportionation of lithium biphenyl in solution: A combined experimental and theoretical study. New J. Chem. *42*, 5168–5177. https://doi.org/10.1039/C7NJ04726F.

76. Yus, M., Herrera, R.P., and Guijarro, A. (2002). On the mechanism of arene-catalyzed lithiation: The role of arene dianions—naphthalene radical anion versus naphthalene dianion. Chem. Eur. J. *8*, 2574–2584. https://doi.org/10.1002/1521-3765(20020603)8:11<2574::AID-CHEM2574>3.0.CO;2-K.

77. Formanuik, A., Ortu, F., Liu, J.-J., Nordaraki, L.E., Tuna, F., Kerridge, A., and Mills, D.P. (2016). Double reduction of 4,4′-bipyridine and reductive coupling of pyridine by two thorium(III) single-electron transfers. Chem. Eur. J. *23*, 2290–2293. https://doi.org/10.1002/chem.201605974.

78. Carrington, A., and dos Santos-Veiga, J. (1962). Electron spin resonance spectra of nitrogen heterocyclic radical ions. Mol. Phys. *5*, 21–29. https://doi.org/10.1080/00268976200100031.

79. Ye, T.N., Park, S.W., Lu, Y.-F., Li, J., Sasase, M., Kitano, M., Tada, T., and Hosono, H. (2020). Vacancy-enabled N_2 activation for ammonia synthesis on a Ni-loaded catalyst. Nature *583*, 391–395. https://doi.org/10.1038/s41586-020-2464-9.

80. Kitano, M., Inoue, Y., Yamazaki, Y., Hayashi, F., Kanbara, S., Matsuishi, S., Yokoyama, T., Kim, S.W., Hara, M., and Hosono, H. (2012). Ammonia synthesis using a stable electride as an electron donor and reversible hydrogen store. Nat. Chem. *4*, 934–940. https://doi.org/10.1038/nchem.1476.

81. Tamaddon, F., and Razmi, Z. (2011). Oxidation of 1,4-dihydropyridines and 3,4-dihydropyrimidin-2(1H)-ones to substituted pyridines and pyrimidinones using $Ca(OCl)_2$ in aqueous media. Synth. Commun. *41*, 485–492. https://doi.org/10.1080/00397911003587523.

82. Memarian, H.R., Abdoli-Senejani, M., and Döpp, D. (2007). Photoinduced aromatization of unsymmetrically substituted 1,4-dihydropyridines. J. Chin. Chem. Soc. *54*, 131–139. https://doi.org/10.1002/jccs.200700022.

83. Zimmerman, H.E. (2012). A mechanistic analysis of the Birch reduction. Acc. Chem. Res. *45*, 164–170. https://doi.org/10.1021/ar2000698.